

Flame Wrinkles From the Zhdanov-Trubnikov Equation.

Guy Joulin^{1#} and Bruno Denet^{2*}

¹ Institut P-prime, UPR 3346 CNRS, ENSMA, Université de Poitiers,
1 rue Clément Ader, B.P. 40109, 86961 Futuroscope Cedex, Poitiers, France.

² Aix-Marseille Univ., IRPHE, UMR 7342 CNRS,
Technopole de Château-Gombert, 49 rue Joliot-Curie, 13384 Marseille Cedex 13, France.

Abstract.

The Zhdanov-Trubnikov equation describing wrinkled premixed flames is studied, using pole-decompositions as starting points. Its one-parameter ($-1 \leq c \leq 1$) nonlinearity generalizes the Michelson-Sivashinsky equation ($c=0$) to a stronger Darrieus-Landau instability. The shapes of steady flame crests (or periodic cells) are deduced from Laguerre (or Jacobi) polynomials when $c \approx -1$, which numerical resolutions confirm. Large wrinkles are analysed *via* a pole density: adapting results of Dunkl relates their shapes to the generating function of Meixner-Pollaczek polynomials, which numerical results confirm for $-1 < c \leq 0$ (reduced stabilization). Although locally ill-behaved if $c > 0$ (over-stabilization) such analytical solutions can yield accurate flame shapes for $0 \leq c \leq 0.6$. Open problems are invoked.

Keywords: Flame pattern, Nonlinearity, Pole decomposition, Integral equation.

1. Introduction.

The flames propagating into premixed gaseous reactants – be they molecular [1] or nuclear [2]– may often be viewed as fronts: their actual thickness ℓ based on flat-flame speed u_L and heat diffusivity often is much smaller than the wavelength of their deformations. Being also very subsonic ($u_L \ll$ speed of sound) such combustion fronts border fluids of constant densities: ρ_u (fresh side) or $\rho_b < \rho_u$. As the Atwood number $\mathcal{A} \equiv (\rho_u - \rho_b) / (\rho_u + \rho_b) < 1$ is nonzero, flames are subject to the hydrodynamic Darrieus [3]-Landau [4] (DL) instability at long wavelengths; at shorter scales, variations in local burning speed (relative to reactants) with front mean curvature provide a neutral wavelength $L_{neutral} \sim \ell$ ($L_{neutral} \gg \ell$, though).

Acknowledging that $\mathcal{A} \ll 1$ implies a weak DL instability, Sivashinsky's analysis [5] provided the first systematic weakly-nonlinear description of the local amplitude Φ of wrinkling: a companion numerical work [6] confirmed that the (Michelson-) Sivashinsky (MS) equation ($c = 0$ in Eq.(1)) correctly captures the slow spontaneous dynamics of flat-on-

guy.joulin@lcd.ensma.fr: Corresponding author, Tel(33)(0)549498186, Fax(33)(0)549498176

* bruno.denet@irphe.univ-mrs.fr

average flames... if $\mathcal{A} \rightarrow 0^+$. Yet in practice \mathcal{A} ranges from 0.2-0.5 (Supernovae) to 0.65-0.85 (chemical fronts), and incorporating higher orders in \mathcal{A} is of interest. The two sub-leading orders just gave the MS equation modified coefficients [7]-[9]. At the next one a new quadratic non-linearity appears in the equation for Φ , but another order only changes coefficients therein [10]. A non-linearity of same type first appeared in $\mathcal{A} = O(1)$ amplitude-expansion derivations of an equation for Φ , where a small flame slope is postulated [11][12].

If a single space coordinate is retained, the Zhdanov-Trubnikov (ZT) type of equation [11] so obtained for slow spontaneous evolutions of front wrinkles has the (rescaled) form:

$$\phi_t + \frac{1}{2}[\phi_x^2 + c \mathcal{H}\{\phi_x\}^2] = \nu\phi_{xx} - \mathcal{H}\{\phi_x\}, \quad (1)$$

where $c = c(\mathcal{A})$, $\phi(t, x) \sim \Phi$ measures the front deformation, and the subscripts denote derivatives with respect to scaled time (t) or coordinate (x). Provided the reference length is suitably chosen, $\nu > 0$ denotes the neutral-to-actual wavelength ratio of *periodic cells*; for *isolated crests*, ν could be rescaled to unity by a change of variables but is kept in (1) for comparisons with cells. Curvature effects gave $\nu\phi_{xx}$ whereas the Hilbert non-local transform $\pi\mathcal{H}\{\phi_x\} := \int_{-\infty}^{+\infty} \phi_x(x')dx'/(x'-x)$ encodes the DL instability: a small $\phi(t, x) \sim \exp(\varpi t + i\kappa x)$ has $\varpi = |\kappa| - \nu\kappa^2$ as growth rate. The stabilizing local nonlinearity in (1) combines geometry [5] and hydrodynamics [7]. The non-local one, absent from the MS equation, mainly is fluid-mechanical [*e.g.* kinetic energy $\sim (\phi_x^2 + \mathcal{H}\{\phi_x\}^2)$]; it may be destabilizing, $c < 0$, or over-stabilizing ($c > 0$), affecting the solutions of (1) in qualitatively different ways (*e.g.* at tips).

Solving the non-linear and non-local Eq.(1) with a general c might help one fit flame shapes from experiments [1], or simulations that use $\mathcal{A} = O(1)$, and is interesting *per se*. The novel solutions of (1), periodic or not, obtained in the present Letter are steps in this direction.

2. Pole decompositions.

Just like the MS equation [13], (1) admits a pole decomposition [14]: $\phi_x(t, z)$, the flame slope continued in complex $z := x + iB$ plane, is meromorphic with simple poles $z_k(t)$. All have $-2\nu/(1-c)$ as residue because of a common dominant balance $\phi_x^2 + c \mathcal{H}\{\phi_x\}^2 \approx 2\nu\phi_{xx}$ at $z \approx z_k(t)$. They feature in N conjugate pairs $z_{-k} = \bar{z}_k$ [$\phi(t, z)$ is real when z is] and obey $2N$ coupled differential equations [dB_k/dt is added to the r.h.s. of (3)(6)] for (1) to be

satisfied [14]. Attention is presently restricted to steady flame shapes. Only two types thereof are to be considered, 2π -periodic cells and non-periodic isolated crests, both of which have their poles aligned along the imaginary axis, $z_k = iB_k \pmod{2\pi}$ in periodic cases); by convention, $B_k < B_{k+1}$ and $\text{sgn}(B_k) = \text{sgn}(k)$. A single alignment (and flame tip) per cell wavelength is chosen for simplicity, and because such patterns constitute attractors when the unsteady (1) is solved with periodic boundary conditions.

Periodic cells with tips centred at $x = 0 \pmod{2\pi}$ have $\phi(t, x) = -Vt + \phi(x)$ and:

$$\phi_x(x) = \frac{-V}{1-c} \sum_{k=-N}^N \cot\left[\frac{1}{2}(x - iB_k)\right]. \quad (2)$$

For the ‘‘steady’’ ZT equation to be fulfilled the $B_{|k|\geq 1}$ ’s must obey [14]

$$v \sum_{j=-N, j \neq k}^{j=N} \frac{1 - c\varepsilon_k \varepsilon_j}{1 - c} \coth\left[\frac{1}{2}(B_k - B_j)\right] = f \varepsilon_k, \quad (3)$$

$$f := 1 + 2vNc / (1 - c), \quad (4)$$

where $\varepsilon_k := \text{sgn}(B_k)$ originates from $\mathcal{H}\{\cot(\frac{1}{2}(x - iB_k))\} = -1 - i\varepsilon_k \cot(\frac{1}{2}(x - iB_k))$. The number N of pole pairs in (2) is constrained by the inequality $\coth(\frac{1}{2}(B_N - B_{j \neq N})) \geq 1$ to be less than $N_{opt}(v) := \lfloor \frac{1}{2}(1 + \frac{1}{v}) \rfloor$ ($\lfloor \cdot \rfloor =$ integer part), but is otherwise arbitrary. The speed $V = (1+c) \frac{1}{2\pi} \int_0^\pi \phi_x^2 dx$ is found [14] from (2)(3) to be $V = 2Nv(1 - Nv) / (1 - c)$, whereby $c^2 \leq 1$.

Centred *Isolated crests* are limiting cases of cells ($z \sim Nv \ll 1$), have $\mathcal{H}\{\phi_x\} \sim v^2 N^2 / x^2 \sim \phi_x^2$ at $|x|/vN \rightarrow \infty$, and $V = 0$. For any $N \geq 1$ they obey ‘local’ versions of (2)-(4), viz.:

$$\phi_x(x) = \frac{-v}{1-c} \sum_{k=-N}^N \frac{2}{x - iB_k}, \quad (5)$$

$$v \sum_{j=-N, j \neq k}^{j=N} \frac{1 - c\varepsilon_k \varepsilon_j}{1 - c} \frac{2}{B_k - B_j} = \varepsilon_k. \quad (6)$$

As when $c = 0$ [13], the only known exact result is then obtained by summing (6) times- B_k over $k \geq 1$, $0 < B_1 + \dots + B_N = vN(2N / (1 - c) - 1)$, whereby $c < 1$.

3. Isolated crests.

For reasons that shall gradually emerge, isolated crests with $c < 0$ are considered first. The simplest of them has $N = 1$. Equation (6) then gives $B_1 / v = (1 + c) / (1 - c)$, with three

consequences: (i) $B_1 > 0$ needs $c^2 < 1$, confirming this range as the physical one; (ii) B_1 / ν increases with c ; (iii) $B_1 / \nu \rightarrow 0$ as $c \rightarrow -1$, suggesting this is a limit to envisage first.

3.1: The $c \rightarrow -1$ limit.

A small $1+c$ means that the $B_{k>0}$ only little feel their ‘‘conjugates’’ $B_{k<0}$... unless very close; yet the exception can only concern $B_{\pm 1}$, due to the repulsion between B_k ’s of like signs. One then anticipates that $B_{\pm 1} / \nu$ will be $O(1+c) \ll 1$, just like when $N = 1$, the other poles staying at finite distances. Under this working assumption (6) simplifies considerably for $k = 2, \dots, N$:

$$2 \sum_{j=2, j \neq k}^{j=N} \frac{\nu}{B_k - B_j} + \frac{\nu(1+\alpha)}{B_k} \approx 1, \quad \alpha = 1. \quad (7)$$

According to a classical work of Stieltjes [15] such leading order $B_{k \geq 2} / \nu := \eta_k$ therefore are zeros of the associated Laguerre polynomial $\mathcal{L}_{N-1}^{(\alpha=1)}(\eta)$. Equation (6) also simplifies for $k = 1$:

$$\frac{(1+c)\nu}{2B_1} \approx 1 + 2 \sum_{j=2}^N \frac{\nu}{B_j}. \quad (8)$$

Since $1/\eta_2 + \dots + 1/\eta_N = \frac{1}{2}(N-1)$ by (7), $B_1 / \nu \approx (1+c)/2N$: as anticipated $B_1 / \nu \ll \eta_2$. On integration (5) then yields the limiting flame shape $\phi(x)$ for $c \rightarrow -1$, uniformly in x and N , in the Hopf-Cole -like form:

$$\phi = \phi^+(x) + \phi^-(x) + \text{const.}, \quad (9)$$

$$(1-c)\phi^\pm(z) = -2\nu \ln[\psi^\pm(z)], \quad (10)$$

where $\nu\psi^\pm(z) = (z \mp iB_1)\mathcal{L}_{N-1}^{(1)}(\pm z / i\nu)$. Numerical resolutions of (6) confirm this: for $N = 10$, $1/\nu = 1/20.5$, $c = 0.999$ they give $B_1 = 2.445 \cdot 10^{-6}$, $B_2 = 0.01799$, $B_6 = 0.3525$, $B_{10} = 1.3722$, while the values predicted from (7)(8) are $2.441 \cdot 10^{-6}$, 0.01796 , 0.3523 , 1.3716 , respectively.

The above steady $\phi(x)$ has a 2-scale structure, $x/\nu \sim 1$ and $x/\nu \sim (1+c)/N \ll 1$. This has counterparts for unsteady shapes $\phi(t, z) = \phi^+(t, z) + \phi^-(t, z)$, with $\phi^-(t, z) = \overline{\phi^+(t, \bar{z})}$ as in (9), and ϕ_z^+ analytic in $\Im(z) \leq 0$ whereby $\mathcal{H}\{\phi_x^\pm\} = \mp i\phi_x^\pm$. Insofar as their lowest poles $iB_{\pm 1}(t)$ have $NB_{\pm 1}(t)/\nu \gg (1+c)$, $(\phi^\pm)_{c \rightarrow -1}$ follow *uncoupled* Burgers-type (thus linearisable) equations

$$\phi_t^\pm + \phi_z^{\pm 2} \mp i\phi_z^\pm = \nu\phi_{zz}^\pm, \quad (11)$$

since well separated poles $iB_k(t)$ with k 's of unlike signs do not interact if $c \rightarrow -1$. Those of ϕ^+ (or ϕ^-) globally drift towards $\Im(z) = 0$ while interacting among themselves, until $NB_{\pm 1}(t) \sim \nu(1+c) \ll 1$. From then on, $F^\pm := \phi^\pm + \nu \ln(z \mp iB_1(t))$ obey another linearisable equation

$$F_t^\pm + F_z^{\pm 2} \mp iF_z^\pm - \frac{2\nu}{z}(F_z^\pm - F_z^\pm(t,0)) = \nu F_{zz}^\pm \quad (12)$$

at all $|z| \gg B_1(t)$ scales. The near-real $B_{\pm 1}(t)$ induce the $\frac{-2\nu}{z}$ ‘‘convection’’ term in (12), and soon get themselves slaved to $F_z^+(t,0) = -F_z^-(t,0)$, $(1+c)\nu/2B_{\pm 1}(t) \approx \pm 1 - 2F_z^\pm(t,0)$ (see (8)). The front shape is then $\phi(t,x) \approx -\nu \ln[(x^2 + B_1(t)^2) |F^+(t,x)|^2]$; it has a spike on top of the smoother pattern governed by (12) that *in fine* monitors its varying height and width.

3.2: Large crests.

Steady poles get packed when $N \rightarrow \infty$, $B_{k+1} - B_k \ll B_N$; it is then appropriate to define such a density $\rho(B) = \rho(-B)$ that $\rho(B)dB$ measures the number of poles with ‘altitudes’ in $(B, B+dB)$ [13]. In this continuous approximation of (6) the pole density pertaining to isolated crests obeys the singular integral equation:

$$\oint \frac{[1 - c\varepsilon(B)\varepsilon(B')]2\nu\rho(B')dB'}{(1-c)(B-B')} = \varepsilon(B), \quad (13)$$

with $\varepsilon(B) := \text{sgn}(B)$. The principal-part prescription of this integral reflects the constraint $j \neq k$ in (6), and its unspecified integration range is unknown; as when $c = 0$ one anticipates that $\rho(|B| > B_{\max}) = 0$ for some $B_{\max} > 0$.

When $c = 0$ Eq.(13) was solved [16] by Fourier series methods in terms of an angle $-\pi/2 \leq \theta \leq \pi/2$ defined by $B/B_{\max} = \sin(\theta)$. The solution $\rho_{c=0}(B)$ reads:

$$2\nu\pi\rho_{c=0} = w(\theta), \quad (14)$$

$$\pi w(\theta) := \ln(\cot^2(\frac{1}{2}\theta)) \quad (15)$$

The normalization $\int_0^{B_{\max}} \rho_{c=0}(B)dB = N$ fixed $B_{\max,c=0}$ to be $2\pi N\nu$ and contour evaluation of

$$\phi_x(x) = \frac{-2\nu}{(1-c)} \int_{-B_{\max}}^{B_{\max}} \frac{\rho(B)dB}{x-iB} \quad (16)$$

with $c = 0$ gave the front slope [16], see below (22). A noteworthy point is as follows: although this density has $-B_{\max} < B < B_{\max}$ as a support, it may be viewed as the restriction to the physical range $-\pi/2 \leq \theta \leq \pi/2$ of a 2π -periodic function $\tilde{\rho}(\theta)$ defined for *all* real θ

and vanishing at all odd multiples of $\pi/2$: this odd continuous function of $w(\theta) = w(-\theta)$ may also be assumed to satisfy:

$$\tilde{\rho}(\theta + 2\pi) = \tilde{\rho}(\theta) = \tilde{\rho}(-\theta) = -\tilde{\rho}(\pi - \theta). \quad (17)$$

We anticipate that such symmetries still hold when $c \neq 0$. Trigonometric identities [e.g. $2 \cos \theta' / (\sin \theta' - \sin \theta) \equiv \cot(\frac{\theta' - \theta}{2}) - \tan(\frac{\theta' + \theta}{2})$] then indicate that (13) will be solved when one finds a $\tilde{\rho}(\theta)$ obeying (17) and

$$\tilde{\varepsilon}(\theta) \mathcal{H}\{\tilde{\rho}(\theta)\} - c \mathcal{H}\{\tilde{\varepsilon}(\theta)\tilde{\rho}(\theta)\} = -(1-c) / 2\pi\nu, \quad (18)$$

where $\tilde{\varepsilon}(\theta) := \text{sgn}(\sin(\theta))$ and the (periodic-) Hilbert transform $\mathcal{H}\{.\}$ now refers to θ .

Not being of the convolution type if $c \neq 0$ (18) is no longer simply amenable to a Fourier method. One can fortunately invoke results by Dunkl [17], who exhibited a sequence of one-variable real polynomials $p_j(\omega)$ that obey ‘‘ladder’’ relations ([17], p.149, Theorem 1) once evaluated at $\omega = w(\theta)$:

$$\mathcal{H}\{\tilde{\varepsilon}(\theta)p_j(w(\theta))\} = +p_{j+1}(w(\theta)), \quad j = 0, 1, \dots, \quad (19)$$

$$\tilde{\varepsilon}(\theta)\mathcal{H}\{p_j(w(\theta))\} = -p_{j-1}(w(\theta)), \quad j = 1, 2, \dots. \quad (20)$$

Direct substitution in (18) and a term-by-term use of (19)(20) show that $2\pi\nu\tilde{\rho}(\theta)/(1-c) = \sum_{n=0}^{\infty} (-c)^n p_{2n+1}(w(\theta))$ satisfies (18) if $p_0(\cdot) = 1$. The $p_j(\omega)$ ’s so identified are the (non-monic) symmetric Meixner-Pollaczek polynomials $P_j^{(\lambda=1/2)}(\omega)$, with $(-1)^j$ as parity and $\sum_{j=0}^{\infty} r^j p_j(\omega) := G(\omega, r) = (1+r^2)^{-1/2} e^{\omega \arctan(r)}$ as generating function [15, 17].

The sum $\sum_{n=0}^{\infty} (r^2)^n p_{2n+1}(\omega)$ is thus $\frac{1}{2r}(G(\omega, r) - G(-\omega, r)) = \frac{(1+r^2)^{-1/2}}{r} \sinh(\omega \arctan(r))$. With $r^2 = -c$ and $\omega = w(\theta)$ this yields $2\pi\nu\tilde{\rho}(\theta)/(1-c)$ in closed form, to produce:

$$2\nu\pi\rho(B) = \frac{(1-c)^{1/2}}{\sqrt{-c}} \sinh\left[w(\theta) \arctan(\sqrt{-c})\right] \quad (21)$$

if specialized to the physical range; as $w(\theta)$ itself (21)obeys (17), and resumes (14) for $c = 0$.

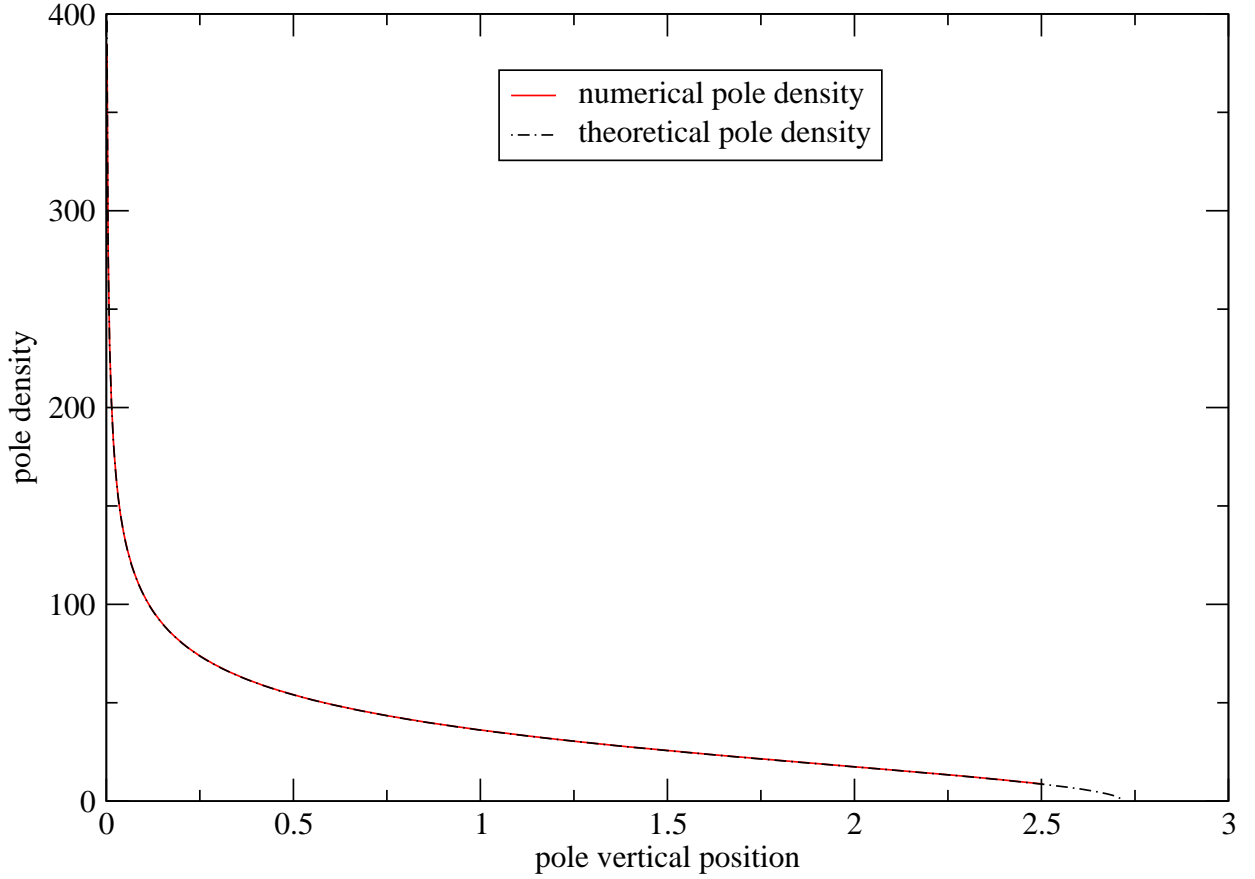


Figure 1: Numerical density [defined by $\rho_{num}(\frac{1}{2}(B_k + B_{k-1})) := 1/(B_k - B_{k-1})$ with B_k 's for crests from (6)] vs. pole altitude B , and predicted density (21); $N = 100$, $\nu = 1/199.5$, $c = -0.25$.

Normalisation requires $B_{\max} \int_0^{\pi/2} \rho(\theta) \cos(\theta) d\theta = N$: contour integrations¹ yield $B_{\max} = 2\nu N \sin(\pi\mu) / \mu$, $0 \leq \cos(\pi\mu) := (1+c)/(1-c) \leq 1$. This and $\theta := \arcsin(B/B_{\max})$ complete the determination of $\rho(B)$ in (21). For $c = -1$, $2\pi\nu\rho$ acquires the Marchenko-Pastur form $(4\pi\nu/|B|-1)^{1/2}$ pertaining to $\mathcal{L}_{N-1 \rightarrow \infty}^{(1)}(|B|/\nu)$ [18], as expected (Sec. 3.1).

¹ This integral reads $\int_0^1 h(t) dt$, $t := \tan(\frac{1}{2}\theta)$, or $\frac{1}{2} \int_0^\infty h(t) dt$ as $h(1/t) \equiv t^2 h(t)$. Integrations by parts then along the contour $\{\Im(u) = 0\} \cup \{\Im(u) = 2\pi\}$ in the complex plane of $u = \ln(t^2)$, and residue evaluations, give B_{\max} .

The flame slope, Eq.(16), is expressible in terms of $\sinh(\xi) := x / B_{\max}$ as:

$$\phi_x(x) = \frac{\text{sgn}(-x)}{2 \tan(\frac{1}{2} \pi \mu)} \left[\left| \coth(\frac{1}{2} \xi) \right|^\mu - \left| \tanh(\frac{1}{2} \xi) \right|^\mu \right], \quad (22)$$

which when $c = 0 = \mu$ resumes the profile $\pi \phi_x(x) = \text{sgn}(-x) \ln \left[\coth^2(\frac{1}{2} \xi) \right]$ found in [16].

Figures 1-3 compare (21)(22), and ensuing flame shapes $\phi(x)$, with what Eqs. (6)(5) give if $N \gg 1$, respectively: smaller $c < 0$ (weaker non-linear stabilization) give sharper crest *tips*.

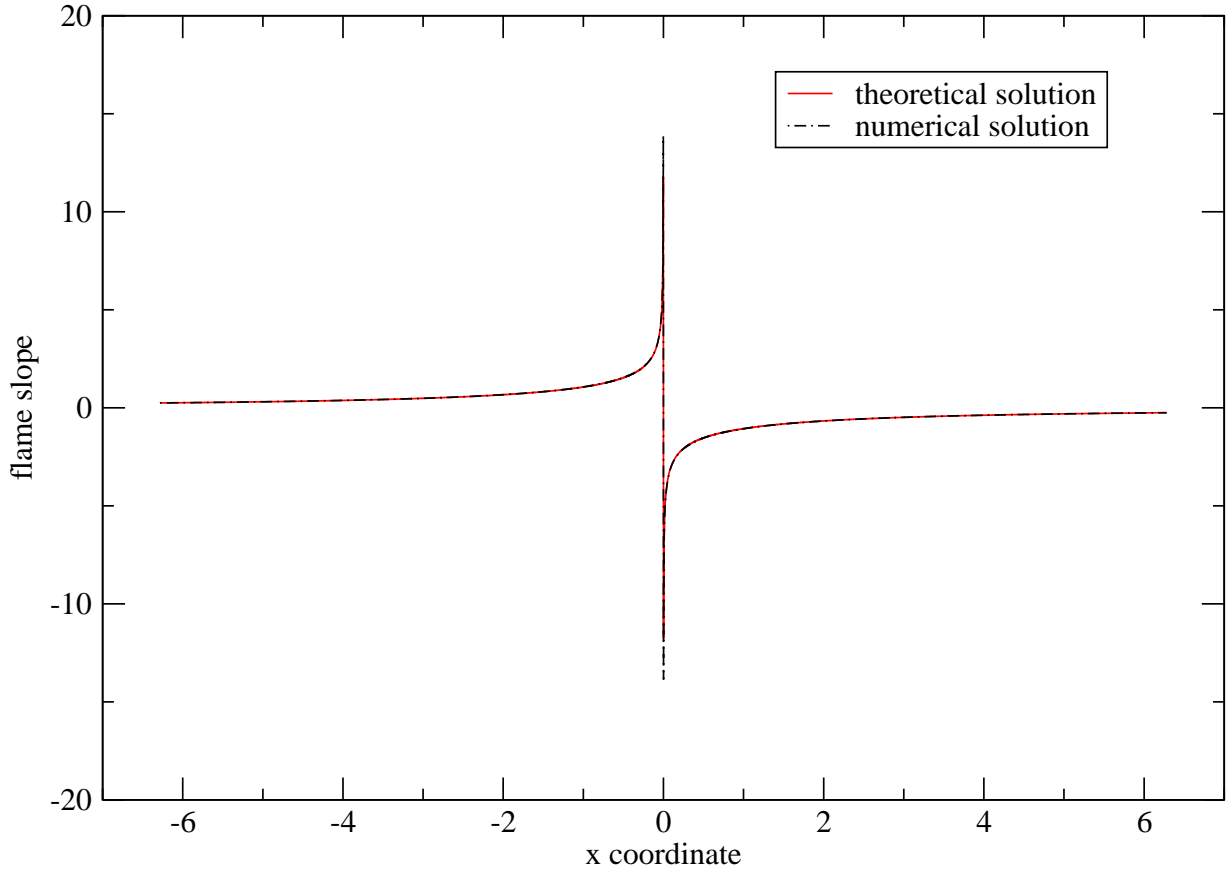


Figure 2: Numerical flame-crest slope $\phi_x(x)$ [from (5)(6)] vs. abscissa x , compared with analytical prediction (22); $N = 100$, $\nu = 1/199.5$, $c = -0.25$.

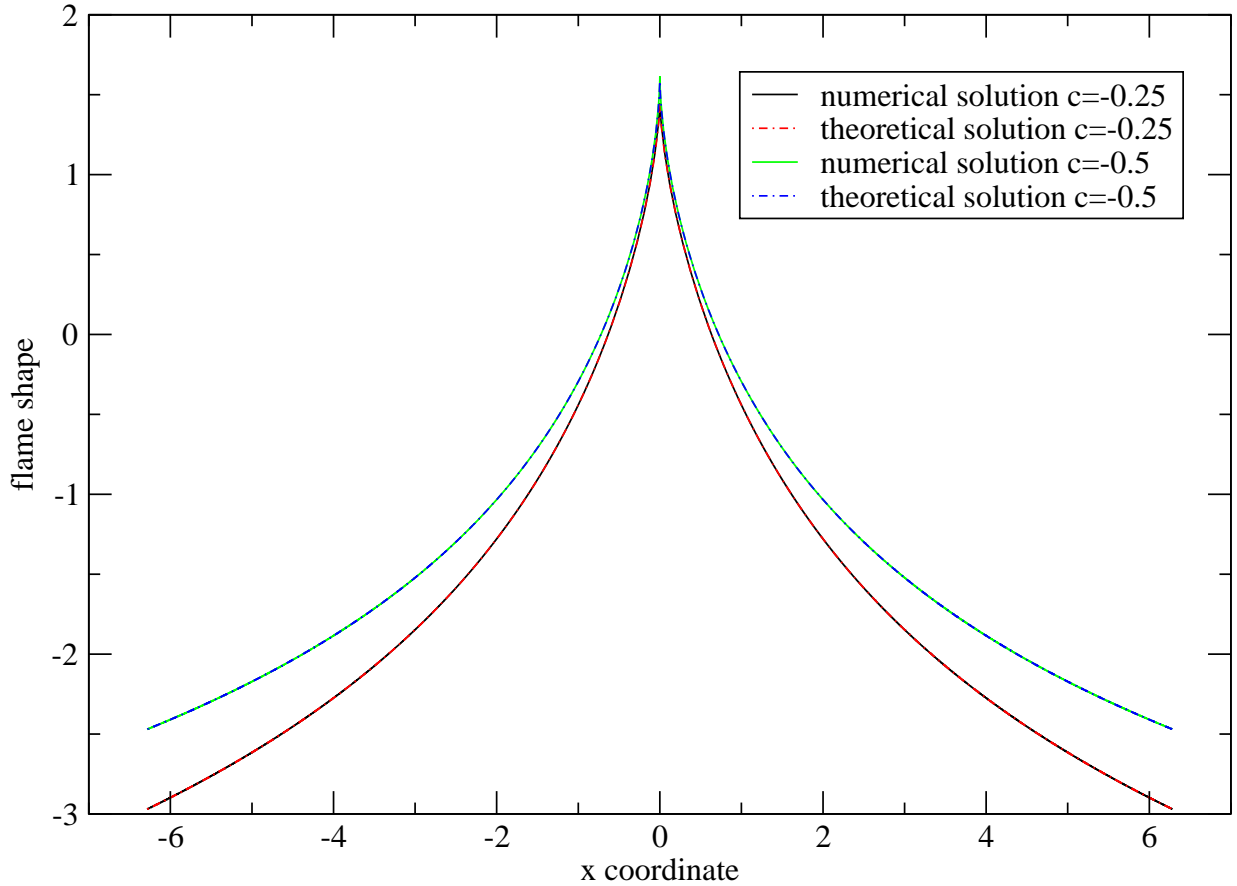


Figure 3: Numerical flame-crest shapes $\phi(x)$ [from (5)(6)] vs. abscissa x [same parameters as in Fig.1], and predictions from numerical quadrature of Eq.(22).

4. Periodic cells.

To analyse 2π -periodic patterns one again starts with $N=1$, in which case (3)(4) give $\tanh(B_1) = \nu(1+c)/(1-c)f$. One checks that $0 < B_1 < \infty$ needs $c^2 < 1$ and $1 = N \leq \frac{1}{2}(1 + \frac{1}{\nu})$, *i.e.* $\nu \leq 1$: cells of finite amplitude exist *iff* unstable modes fit in the box $|x| < \pi$.

4.1: The $c \rightarrow -1$ limit.

$B_1 > 0$ again is well below B_2, \dots, B_N if $0 < 1+c = o(1)$. Equations (3)(4) specialized to the latter poles again simplify, especially when expressed in terms of $C_k := \coth(\frac{1}{2}B_k) > 1$:

$$\sum_{j=2, j \neq k}^{j=N} \frac{\nu(1-C_k^2)}{(C_k - C_j)} + \nu(N-1)C_k - 1 - \frac{2N\nu c}{1-c} \approx 0. \quad (23)$$

Another result of Stieltjes [15] says that such C_k 's coincide with the zeros of a Jacobi polynomial $P_{N-1}^{(\alpha_1', \alpha_1'')}(C)$ in $C := \coth(\frac{1}{2}B)$, yet with indices $\alpha_1' = 1/\nu - 2N$ and $\alpha_1'' = -1/\nu < 0$ that lead to nonstandard polynomials ($\alpha_1'' < -1$). The identity $P_{N-1}^{(\alpha_1', \alpha_1'')}(X_1)/(1+X_1)^{N-1} \sim P_{N-1}^{(\alpha_2', \alpha_2'')}(X_2)$, with $X_2 = (3-X_1)/(1+X_1)$, $\alpha_2' = \alpha_1'$, $\alpha_2'' = 1-2N-\alpha_1'-\alpha_1''$ [19], and another identity changing the first index only, fortunately help one access the $C_{k \geq 2} > 1$: they obey the more manageable $P_{N-1}^{(\alpha', \alpha'')((C-3)/(C+1))} = 0$, where $\alpha' = 1$ and $\nu\alpha'' = 1-2N\nu \geq 0$. Equation (3) also simplifies for $k=1$, giving $B_1 \approx \nu(1+c)/2N(1-N\nu) \ll B_2$ once $C_2 + \dots + C_N = 1/\nu - N$ (by (23)) is used.

The flame shape then obeys (9)(10) with $\psi^\pm(z) = \sin(\frac{1}{2}(z \mp iB_1))P_{N-1}^{(\alpha', \alpha'')}(2e^{\pm iz} - 1)$, since $(C-3)/(C+1) \equiv 2e^B - 1$. The resulting wrinkle amplitude $\max(\phi) - \min(\phi)$ diverges like $-2\nu \ln(1+c) + \text{const.}$ when $c \rightarrow -1$ at fixed ν and $\nu N \sim 1$, because $-\nu \ln\{|\sin(\frac{1}{2}(x-iB_1))|^2\}$ endows the front with spikes centred at $x = 0 \pmod{.2\pi}$, each of $O(B_1) \sim \nu(1+c)/N$ width.

4.2: Large cells.

In the large- N limit the neutral-to-actual wavelength ratio ν must be small, for compatibility with $N \leq N_{opt}(\nu) \approx \frac{1}{2\nu}$. With this proviso, the pole-density $\rho(B)$ now obeys:

$$\oint \frac{[1-c\varepsilon(B)\varepsilon(B')]\nu\rho(B)dB'}{(1-c)\tanh(\frac{1}{2}(B-B'))} = f\varepsilon(B). \quad (24)$$

The identity $\coth(\frac{1}{2}(B-B')) \equiv (1-T^2)/(T-T')-T'$, with $T := \tanh(\frac{1}{2}B)$ and similarly for T' , helps one solve this formidable-looking equation. Trading B for T and exploiting the parities of ρ and $\varepsilon(T) = \varepsilon(B)$ indeed produces:

$$\oint \frac{[1-c\varepsilon(T)\varepsilon(T')]2\nu\rho(T')dT'}{(1-c)(T-T')F} = \varepsilon(T), \quad (25)$$

$$F := 1 + \frac{2\nu Nc}{1-c} - c \int \frac{2\nu\rho(T')T'\varepsilon(T')dT'}{(1-c)(1-T'^2)}, \quad (26)$$

which formally coincides with (13), except for the provisionally unknown constant $F \neq 1$. One can nevertheless transpose the result on isolated crests as:

$$2\nu\pi\rho(B) / F = (1-c)^{1/2} \sinh \left[w(\theta) \arctan(\sqrt{-c}) \right] / \sqrt{-c}, \quad (27)$$

where now $\tanh(\frac{1}{2}B) := \sin(\theta) \tanh(\frac{1}{2}B_{\max})$. The integrals $\int_0^{B_{\max}} \rho(B)dB = N$ and in definition (26) are amenable to contour integrations [again in $\ln(\tan^2(\frac{1}{2}\theta))$ -plane, similar to footnote¹], to ultimately yields all the ingredients needed to characterize $\rho(B)$ in (27):

$$\tanh(\frac{1}{2}B_{\max}) = \sin(\beta), \quad F = \frac{1-c(1-2N\nu)}{\cos(\mu\beta)(1-c)}, \quad (28)$$

$$\tan(\mu\beta) := \frac{2\nu N \sqrt{-c}}{1-c(1-2N\nu)}, \quad \tan(\frac{1}{2}\pi\mu) := \sqrt{-c}. \quad (29)$$

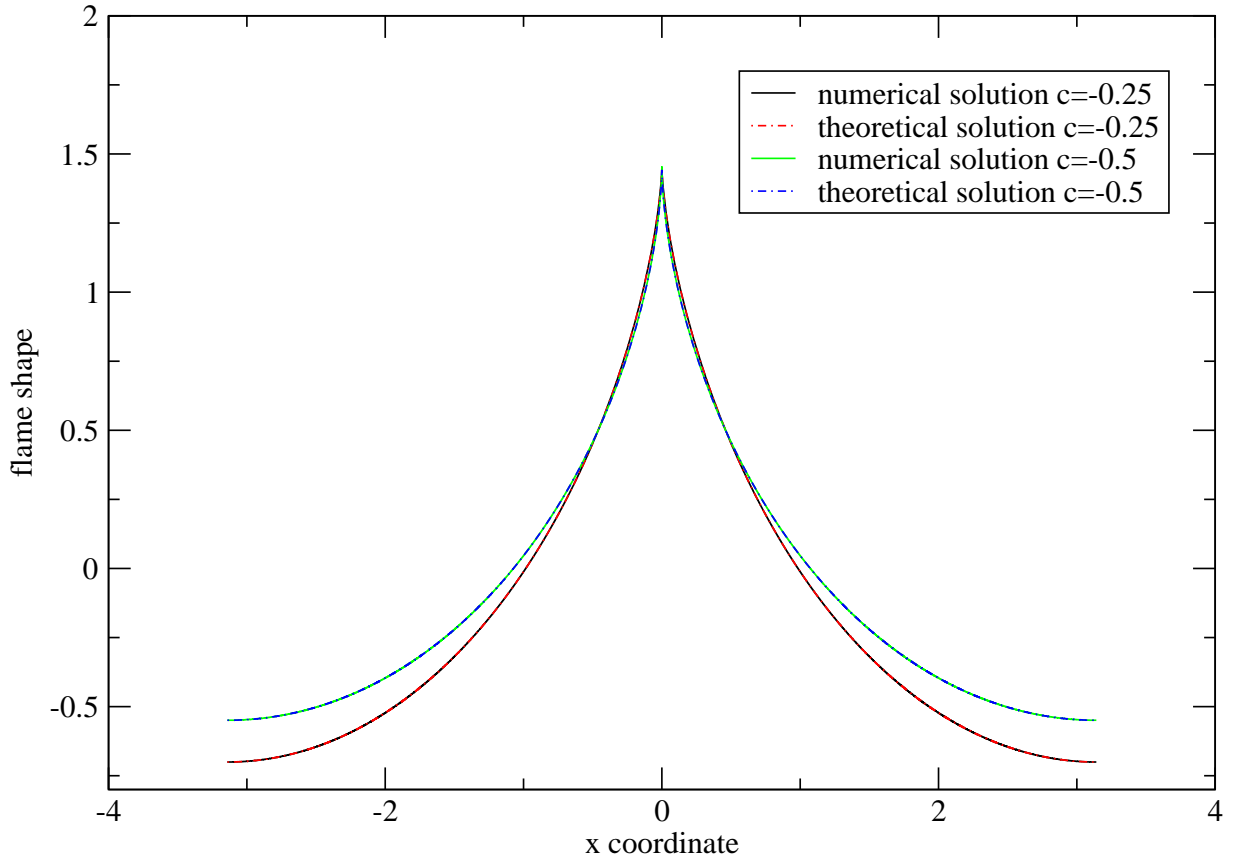


Figure 4: Numerical flame-cell shapes $\phi(x)$ [from (2)(3)] vs. abscissa x [same parameters as in Fig.1], and predictions from quadrature of Eq.(30).

One checks that: (i) $N\nu \ll 1$ gives $B_{\max}/2 \approx \beta \ll 1$, $F \approx 1$ and B_{\max} near to the same $2\nu N \sin(\mu\pi)/\mu$ as for isolated crests; (ii) $B_{\max} = \infty$ if $2\nu N = 1 \approx 2\nu N_{opt}$; (iii) At $c = -1$, $2\pi\nu\rho = (1 - N\nu) \left[\tanh(\frac{1}{2} B_{\max}) / \tanh(\frac{1}{2} B) - 1 \right]^{1/2}$. The flame slope resembles (22):

$$\phi_x(x) = \frac{\text{sgn}(-x)F}{2 \tan(\frac{1}{2} \pi\mu)} \left[1 - \left| \coth(\frac{1}{2} \xi) \right|^\mu - \left| \tanh(\frac{1}{2} \xi) \right|^\mu \right], \quad (30)$$

yet with $\sinh(\xi) = \tan(\frac{1}{2} x) / \tanh(\frac{1}{2} B_{\max})$. When $2\nu N = 1$ [$\beta = \frac{\pi}{2}$, $B_{\max} = \infty$, $\tanh(\frac{1}{2} \xi) = \tan(\frac{1}{4} x)$, $F = \cos(\frac{1}{2} \pi\mu)$] the flame shape is expressible *via* hypergeometric functions ${}_2F_1[\dots]$:

$$\phi(x) = 2(Y(x, \mu) - Y(x, -\mu)) \cos(\frac{1}{2} \pi\mu) / \tan(\frac{1}{2} \pi\mu), \quad (31)$$

where $(1 + \mu)Y(x, \mu) := {}_2F_1\left[1, \frac{1+\mu}{2}; 1 + \frac{1+\mu}{2}; -\tan^2(\frac{1}{4} x)\right] \tan^{1+\mu}(\frac{1}{4} |x|)$.

Numerical resolutions of (3) with $N \gg 1$ confirm the above findings, see Fig. 4: although $c < 0$ implies sharp tips, $[\phi] := -\int_0^\pi \phi_x dx$ decreases as $|c|$ grows. And $[\phi]$ remains finite at $c = -1$: continuous densities cannot capture the sharp spikes caused by $NB_1 = o(\nu)$ (Sec. 4.1).

5. Positive c 's.

The procedure leading to (21)(27) formally applies to $0 < c < 1$ (one may still use the generating function $G(\omega, r)$ with $r^2 = -c$, since $|r| < 1$ [17]): $\sqrt{-c} = ic^{1/2}$ just gets imaginary, as does the exponent $\mu = im$ now related to c by $1 < (1+c)/(1-c) = \cosh(m\pi)$. The pole density (21) previously tailored for isolated crests with $c < 0$ simply becomes:

$$2\nu\pi\rho(B) = (1-c)^{1/2} \sin\left[w(\theta) \operatorname{atanh}(c^{1/2})\right] / c^{1/2}. \quad (32)$$

This $\rho(B)$ wildly oscillates as $|B|$ decreases below $B_{\max} \sin(\theta_0)$, $\tan(\frac{1}{2} \theta_0) := e^{-\pi/m}$, as does $\phi_x(x) = \text{sgn}(-x) \coth(\frac{1}{2} \pi m) \sin\left[m \ln(\coth(\frac{1}{2} |\xi|))\right]$ near $x = 0$: although an exact solution of (13) the above $\rho(B)$ is physically *spurious*, because acceptable pole-densities are nonnegative.

Still, when $c > 0$ is small enough, numerical resolutions of (3) for large isolated crests reveal that the above $\rho(B)$ accurately fits the numerical density defined by $\rho_{num}(\frac{1}{2}(B_k + B_{k-1})) := 1/(B_k - B_{k-1})$, if (32) uses $B_{\max} = 2\nu N \sinh(m\pi)/m$ as $\int_0^{B_{\max}} \rho(B) dB = N$ would imply; the resulting $\phi_x(x)$ very accurately fits the numerical slopes, except *very* close to $x = 0$, Fig.5.

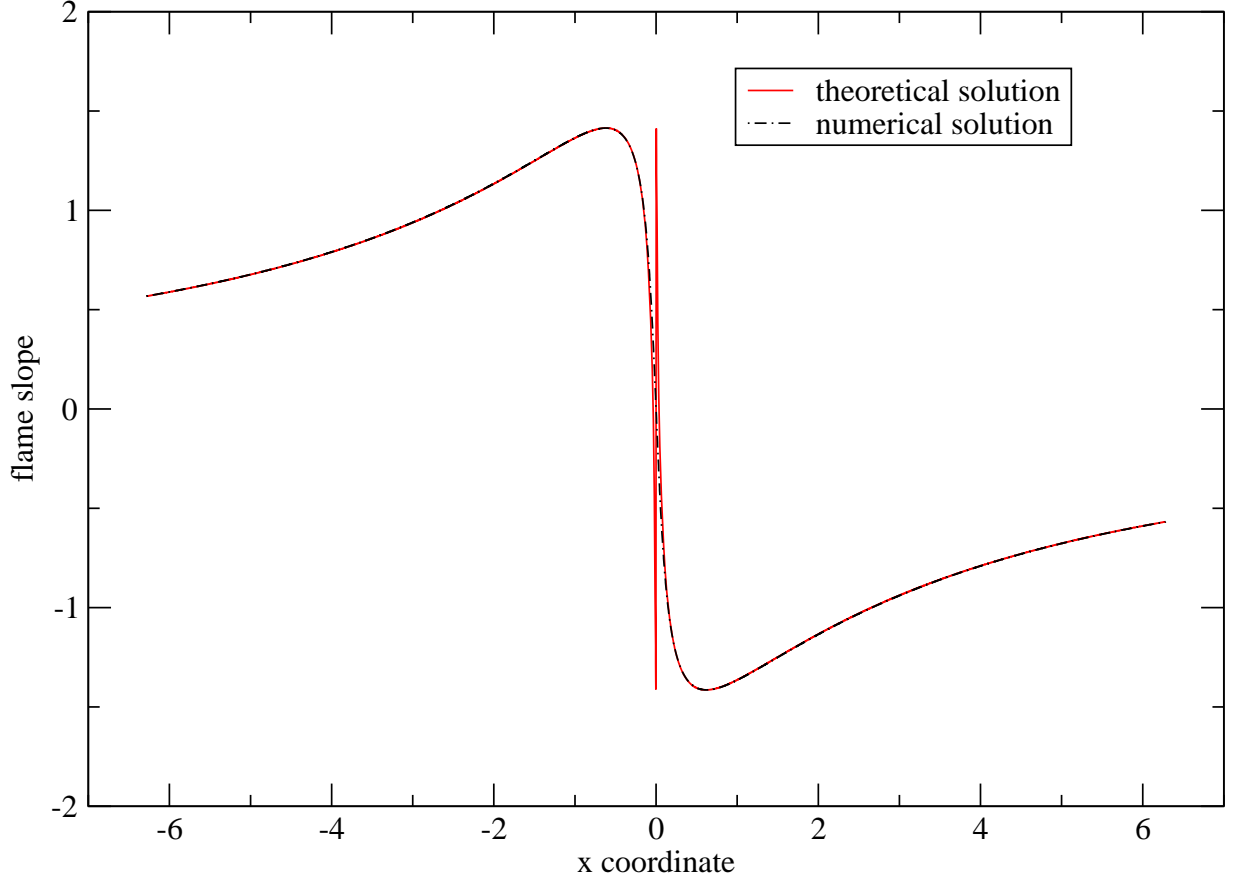


Figure 5: Numerical flame-crest slope [from (5)(6)] vs. abscissa x , and the predicted $\phi_x(x)$ given below Eq.(32); $N = 100$, $\nu = 1/199.5$, $c = +0.5$.

The actual density will vanish for $|B|$ below some $B_{\min} > 0$, however. Nice uniform fits of $\phi_x(x)$ (not shown) result from truncating (32) for $|B| < B_c = B_{\max} \sin(\theta_c)$, with $\int_0^{B_c} \rho dB = 0$ not to alter normalisation: *i.e.*, $\tan(\frac{1}{2}\theta_c) / \tan(\frac{1}{2}\theta_0) \approx e^{\arctan(m)/m} > 1$ if $B_c \ll B_{\max}$. B_c / B_{\max} is effectively small ($\approx 2e^{1-\pi^2/\sqrt{c}}$) if $0 < c \ll 1$ but happens to stay so for $c \lesssim 0.6$ ($e^{-\pi^2/\sqrt{0.6}} \approx 3 \cdot 10^{-6}$). The above $\rho(B)$, ϕ_x and B_{\max} will hopefully yield correct outer solutions at $|x + iB| \gg B_c$, for $c \rightarrow 0^+$. For periodic cells, $\tanh(\frac{1}{2}B_c) \coth(\frac{1}{2}B_{\max}) := \sin(\theta_c)$ has the same, F -independent, θ_c that can also yield good fits.

6. Open problems.

This work provides analytical descriptions of steady flame shapes obeying the Zhdanov-Trubnikov equation (1), mostly when its non-local non-linearity is destabilizing ($c < 0$) and the front wrinkles are sharper than MS flames. Yet some problems remain pending.

The density and front-slope obtained for large wrinkles with $c < 0$ are *outer* solutions that hold for $N \rightarrow \infty$ only at fixed $c \neq 0$ and $z := x + iB = O(B_{\max})$. According to [13], *discrete* pole locations B_j can nevertheless be estimated from $\rho(B)$ by $\int_0^{B_j} \rho(B) dB \approx j - 1/2$: (21) gives $B_j / B_{\max} \sim ((j - 1/2) / N)^{1/(1-\mu)}$ for $0 < j = O(1)$. Although potentially useful to get the tip curvature $\sim 1/B_1$ when N is moderately large, no analysis of the flame-tip region(s) $O(1/N^{1/(1-\mu)}) \leq |z|/B_{\max} \ll 1$ is available.

Although it can yield accurate fits for over-stabilized flames ($c > 0$) up to $c \approx 0.6$, the proposed above density truncation is just an *ad-hoc* stopgap: a bounded-below density support $0 < B_{\min} \leq B \leq B_{\max}$ should instead be introduced from the outset. But alternative methods are needed to handle this, not to mention the flame-tip structure(s) if $1/N$ and $c \geq 0$ are small.

A fuller treatment should also describe the 2-tip wrinkles resembling experiments [1] that (1) *often* produces if endowed with Neumann conditions (2 unlike pole-rows per cell [13] [20]).

References.

- [1] J. Quinard, G. Searby, B. Denet and J. Grana-Otero, *Flow, Turbulence and Combustion*, 87 (2011), Springer, DOI 10.1007/s10494-011-9350-3.
- [2] F.K. Röpke, W. Hillebrandt and J.C. Niemeyer, *Astron. Astrophys.* **420** (2004) 411.
- [3] G. Darrieus, work presented at La Technique Moderne, Paris, 1938, unpublished.
- [4] L. D. Landau, *Acta Physicochim. URSS*, **19** (1944) 77.
- [5] G. I. Sivashinsky, *Acta Astron.* **4** (1977) 1177.
- [6] D. N. Michelson and G.I. Sivashinsky, *Acta Astron.* **4** (1977) 1207.
- [7] P. Clavin and G.I. Sivashinsky, *J. Phys. France*, **48** (1987) 193.
- [8] K.A.Kazakov and M.A.Liberman, *Phys. Fluids*, **14** (2002) 1166.
- [9] K.A. Kazakov, *Phys. Fluids*, **17** (2005) 032107.
- [10] K. A. Kazakov, O. E. Peil and N. A. Pekaľ'n, "Effect of Higher-Order Nonlinearity on the Steady Propagation of Premixed Flames with Weak Gas Expansion", in preparation.

- [11] S. Zhdanov and B. Trubnikov, *J. Exp. Theor. Phys.*, **68** (1989) 65.
- [12] V.V. Bychkov, K.A. Kovalev and M.A. Liberman, *Phys. Rev.* **E 60** (1999) 2897.
- [13] O. Thual, U. Frisch and M. Hénon, *J. Phys. France*, **46** (1985) 1485.
- [14] G. Joulin, *J. Exp. Theor. Phys.*, **100** (1991) 428.
- [15] G. E. Andrews, R. Askey and R. Roy, *Special Functions*, Cambridge University Press, Cambridge, 2000.
- [16] G. Joulin and B. Denet, *Phys. Rev.*, **E 78** (2008) 016315.
- [17] C. F. Dunkl, *Indagationes Mathematicae*, **88**, n°2 (1985) 147.
- [18] S. Shastri and B. Dhar, *J. Phys. A*, **34** (2001), 6197.
- [19] A.B.J. Kuijlaars and A. Martinez-Finkelshtein, *J. Anal. Math.*, **94** (2004) 195.
- [20] B. Denet, *Phys. Rev.* **E 74** (2006) 036303.
